Supplementary Figures and Tables for Simulation and GTP Data Analysis

This section contains additional Figures for simulation studies, a heatmap for the structural connectivity in the GTP data, as well as additional prediction boxplots for GPT data analysis corresponding to different network densities as well as analysis with and without adjusting for BDI (Beck depression index), and Tables that report p-values comparing significant differences in predictive performance for both the BDI adjusted and BDI unadjusted analysis.

For the secondary analysis involving a BDI adjusted prediction of resilience using dynamic networks, we first regressed out the effect for BDI from the resilience score via a linear regression model, and then we used the residuals from these analyses to perform the scalar-on-function regression using the functional connectivity as covariates as in the BDI unadjusted analysis. Both the BDI adjusted and unadjusted analyses results suggest that the dynamic network computed via the proposed mDFC approach still results in significantly improved predictive performance for resilience compared to adjusted regression models that employ the dynamic networks computed under alternative network modeling methods. This is evident from Table 1, and the boxplots for the out of sample predictive accuracy in Figures 8-11. As seen from these Tables and boxplots, the gains in prediction accuracy of the proposed multimodal network modeling approach compared to the alternative network modeling approaches decreases under the BDI adjusted model compared to the BDI unadjusted analysis. A key reason for this difference is the fact that BDI is often significantly associated with PTSD symptoms, so that in some cases, the predictive ability of BDI overshadows the contributions by the dynamic brain network, which results in similar predictive performance under different dynamic network modeling methods under the BDI adjusted analysis.

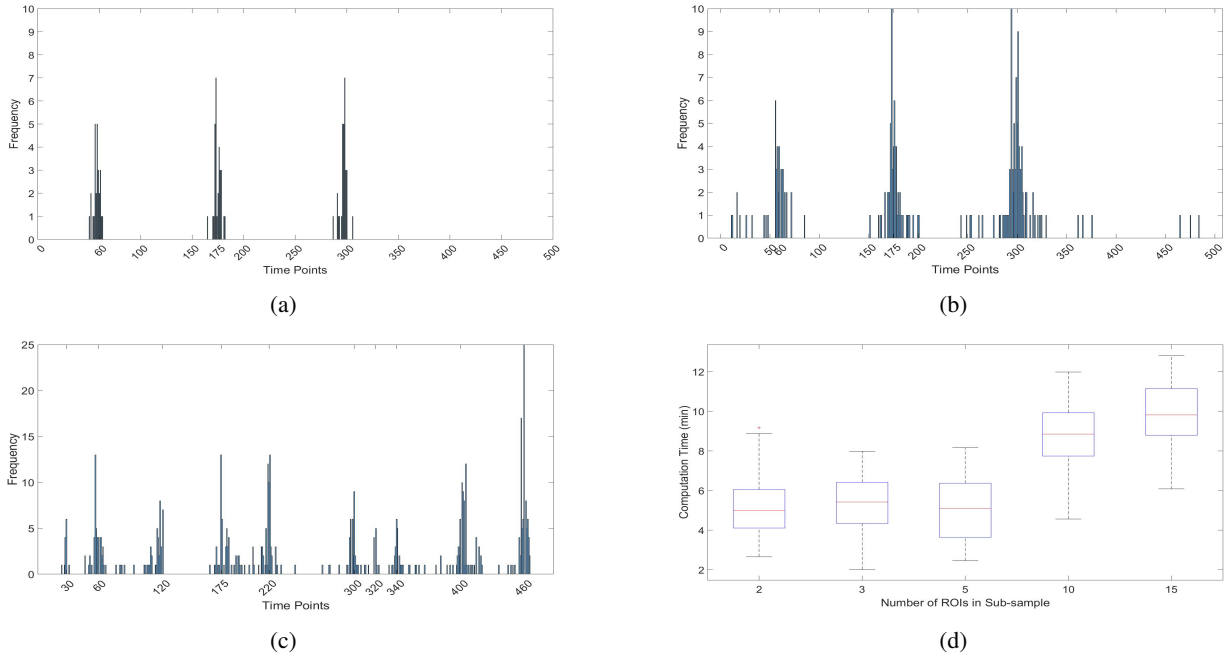

Figure 2. Panels (a)-(c) denote frequency plots for change point estimation. Panels (a) and (b) correspond to the case of $V = 20$ and $V = 100$ nodes respectively, with the true change points being located at 60, 165, and 300. Panel (c) corresponds to the case of 10 true change points which are labeled on the X-axis. The histograms show a strong clustering around true change points. Although there exist some loosely grouped frequencies corresponding to spurious change points, they are almost always eliminated through sub-network sampling mechanism. Panel (d) depicts the computation time as the sub-network size is varied.